

Charged Higgs Production in Association With W^\pm at Large Hadron Colliders

Guo-Li Liu^{1,3}, Fei Wang^{1,3}, Shuo Yang^{2,3}

¹ *Physics Department, Zhengzhou University, Henan, 450001, China*

² *Physics Department, Dalian University, Dalian, 116622, China*

³ *Kavli Institute for Theoretical Physics China, Academia Sinica, Beijing 100190, China*

Many new physics models beyond the standard model (SM) can give rise to the large charged Higgs couplings $H^-q\bar{b}$ and $H^+b\bar{q}$, where $q = t$ or the new vector-like heavy quark T , which are predicted in many new physics models, such as the littlest higgs (LH) models and the left right twin higgs Models (LRTH); On the other hand, some new physics models like the LH also predict the gauge-higgs couplings. Such couplings may have sizable collider phenomenology. We focus our attention on these couplings induced by the LH and the LRTH models and consider their contributions to the production cross section for $W^\pm H^\mp$ production at the LHC. We find that the cross sections in the LH models on the parton level $gg \rightarrow W^\pm H^\mp$ and $q\bar{q} \rightarrow W^\pm H^\mp$ ($q = u, d, s, c, b$) may reach tens of several dozen femtobarns in reasonable parameters space at 14 TeV. The cross section can even reach a few hundred femtobarns in certain favored space. The total cross section of the production $W^\pm H^\mp$ can reach a few hundred femtobarns in quite a large parameter space. While in LRTH, the production rates are basically one order lower than these in LH. Therefore, due to the large cross sections of that in the LH, it may be possible to probe the charged higgs via this process in a large parameter space.

PACS numbers:

I. INTRODUCTION

The primary goal of the Large Hadron Collider (LHC) at CERN is to verify the electroweak symmetry breaking mechanism and discover or rule out the existence of a Higgs boson. Since both the ATLAS and CMS collaborations have discovered a Higgs boson-like particle with mass of around 125 GeV at a significance of 5σ last year, the goal seems to have been reached [1, 2]. Apart from searches for the Higgs boson, there is an ongoing hunting for signals of physics beyond the Standard Model (SM) at the LHC, and hopefully these experiments will shed some light on physics at the TeV scale.

The prediction of a fundamental Higgs boson in the Standard Model appears to be incomplete and reveals aesthetical and theoretical problems such as the famous hierarchy problem and triviality problem. Various new physics models beyond the Standard Model can solve in different ways the previous mentioned problems. In the Little Higgs models, the Higgs bosons emerges as the pseudo Nambu-Goldstone bosons associate with the spontaneous breaking of a global symmetry. In order to implement the collective symmetry breaking mechanism, new particles such as heavy gauge bosons and top-partners are introduced. Quadratically divergent corrections contributed by such new particles to Higgs boson masses cancel out those by the top quark and gauge boson loops at one-loop level. Thus no much fine tuning is needed in Little Higgs model with cut off scale $\mathcal{O}(10\text{TeV})$. Another example is the left-right twin higgs model. Again, the Higgs bosons in nature are pseudo-Goldstone bosons from spontaneously broken global symmetry. Gauge and Yukawa interactions that explicitly break the global symmetry can give masses to the Higgs bosons.

As a consequence of the discrete twin symmetry, the quadratic terms in the Higgs potential respect the global symmetry, thus does not contribute to the Higgs masses. However, logarithmically divergent terms are radiatively generated which are not invariant under global symmetry and contribute a mass to the pseudo-Goldstones. The resulting Higgs mass is around the electroweak scale when the cut off is around $5 \sim 10$ TeV. The twin Higgs mechanism can be implemented in left-right models with the discrete symmetry being identified with left-right symmetry.

Little higgs models and the left-right twin higgs models predict multiplet physical Higgs bosons, two of which are charged. Since it is hard to distinguish between the CP-even higgs bosons in such new physics models and the higgs boson in the standard model, observation of a charged Higgs is a crucial signature for new physics beyond the standard model. That is why the charged scalar particles have attracted much attention in the previous years by different high energy physics experiments and they will certainly be probed on LHC.

The search for Higgs bosons and new physics particles and the study of their properties are among the prime objectives of the large hadron collider (LHC) [3]. Since the discovery of the charged Higgs bosons will be the evidence of new physics beyond the SM, there are increasing interests in theoretical and experimental studies to provide the basis for its accurate exploration. Therefore the LH and LRTH models are very interesting since in these models charged scalars are predicted and they may possess larger tree-level or one-loop top or bottom Yukawa couplings so we may detect the new Yukawa coupling in these models, which may serve as a sensitive probe of the two models.

Much effort is put in the search for charged Higgs bosons. There is a direct detection limit $M_{H^\pm} > 78.6$ GeV from

the LEP searches through its exclusive decay modes $H^\pm \rightarrow \tau\nu$ and $H^\pm \rightarrow cs$ [4, 5]. The main discover channel for charged Higgs bosons at the hadron collider differ with respect to their mass range. For charged Higgs fields in the low mass range $m_{H^\pm} < m_t$, the signal for such charged Higgs boson is from top quark decay $t \rightarrow H^\pm b$ followed by the decay $H^\pm \rightarrow \tau\nu_\tau$. At the Tevatron, due to phase space suppression for a heavy charged Higgs boson production, the search is mainly focused on the low mass range $m_{H^\pm} < m_t$. Currently there is no charged Higgs signal detected from top decay nor obvious deviation from Wtb vertex measurement, which can put a constraint to THDM on the small and large $\tan\beta$ regions for a charged Higgs boson mass up to ~ 160 GeV [6]. However, due to the large CME for LHC, the search for a heavy charged Higgs boson can be feasible via the $gb \rightarrow tH^-$ production up to a large mass range [7]. For the large mass range $m_{H^\pm} > m_t$, the signal is from the main production process the gb fusion ($gb \rightarrow tH^-$) followed by its decays. When a charged Higgs boson is heavy enough, its main decay mode can be $H^- \rightarrow t\bar{b}$ while other modes (say $H^- \rightarrow \tau\nu_\tau$) are small and can be neglected. So the light charged Higgs ($m(H^\pm) < 175$ GeV) is produced from the top pair production while the heavy charged Higgs ($m(H^\pm) > 175$ GeV) is produced through $gg \rightarrow t\bar{b}H^-$ and $gb \rightarrow tH^-$ with a combination procedure described in Refs. [8] and [9].

When the heavy charged Higgs boson is around 1TeV or higher, the top quark from its decay can be highly boosted and the detectors of LHC may not resolve all jets from its decay when the angle separation parameter is fixed to a specific value (say $R = 0.5$ in anti-kt jet algorithm). Recently, motivated by new technique of ‘‘jet substructure’’ [10–14] developed for highly boosted massive particles, a ‘‘hybrid-R reconstruction method’’, which can use the top tagging and the b tagging for other isolated b jets as well as the full reconstructed objects in the final state to suppress the background, is proposed to investigate the full hadronical decay channel of the heavy charged Higgs production.

Recently, discussions on neutral or charged Higgs production at the LHC have been carried out, see e.g, Refs [15–20]. Both the little Higgs models[21] and the left-right twin Higgs models [22] predict neutral or charged (ϕ^0, ϕ^\pm or H^\pm) scalars with large Yukawa couplings to the third generation quarks in addition to a SM-like Higgs. They also predict one vector-like heavy top quark T and new gauge bosons (A_H, Z_H, W_H). Such new particles can be regarded as a typical feature of those models. Signals of this two models have already been studied in the work environment of linear colliders and hadron-hadron colliders [23], but most attentions had been concentrated on the neutral scalars and new gauge bosons. Here we wish to discuss the aspects of the charged scalars.

For the production of charged top pion in association with a W boson at the LHC, there are mainly two kinds of the partonic subprocesses that contribute to the hadronic cross section $pp \rightarrow W^\pm \phi^\mp$: the $q\bar{q}$ ($q = u, d, c, s, b$) annihilation and the gg fusion. In this paper we shall discuss the production of charged scalar ϕ^\pm in association with SM gauge bosons W^\mp via those two kinds subprocesses, including the contributions arising from neutral and charged scalar, the SM-like Higgs H and the gauge bosons, to search for new physics particles and test these model.

This work is organized as follows. In Sec. II we recapitulate the LH models, give the couplings relevant to our discussion and then discuss the numerical results in it. Similarly, in Sec. III the LRTH models are simply described and the numerical results will be given. Finally, we compare the results predicted by the two models and give our conclusion in Sec. IV.

II. THE LH MODEL AND $W^\pm H^\mp$ PRODUCTION AT THE LHC

A. The LH model and the relative couplings

The littlest Higgs model[24] is based on the $SU(5)/SO(5)$ nonlinear sigma model. At the scale $\Lambda_s \sim 4\pi f$, the global $SU(5)$ symmetry is broken into its subgroup $SO(5)$ via a vacuum condensate f , resulting in 14 Goldstone bosons. The effective field theory of these Goldstone bosons is parameterized by a non-linear σ model with gauged symmetry $[SU(2) \times U(1)]^2$, spontaneously broken down to its diagonal subgroup $SU(2) \times U(1)$, identified as the SM electroweak gauge group. Four of these Goldstone bosons are eaten by the broken gauge generators, leaving 10 states that transform under the SM gauge group as a doublet H and a triplet Φ . This breaking scenario also gives rise to four massive gauge bosons A_H, Z_H and W_H^\pm .

The leading order dimension-two term in the non-linear σ -model can be written for the scalar sector as [24]

$$\mathcal{L}_\Sigma = \frac{1}{2} \frac{f^2}{4} \text{Tr} |\mathcal{D}_\mu \Sigma|^2. \quad (1)$$

The numerical coefficients have been chosen so that the scalar kinetic terms are canonically normalized. The covariant derivative is defined as

$$\mathcal{D}_\mu \Sigma = \partial_\mu \Sigma - i \sum_{j=1}^2 (g_j (W_j \Sigma + \Sigma W_j^T) + g'_j (B_j \Sigma + \Sigma B_j^T)). \quad (2)$$

To linearize the theory, one can expand Σ in powers of $1/f$ around its vacuum expectation value Σ_0

$$\Sigma = \Sigma_0 + \frac{2i}{f} \begin{pmatrix} \phi^\dagger & \frac{h^\dagger}{\sqrt{2}} & \mathbf{0}_{2 \times 2} \\ \frac{h^*}{\sqrt{2}} & 0 & \frac{h}{\sqrt{2}} \\ \mathbf{0}_{2 \times 2} & \frac{h^T}{\sqrt{2}} & \phi \end{pmatrix} + \mathcal{O}\left(\frac{1}{f^2}\right), \quad (3)$$

where h is a doublet and ϕ is a triplet under the unbroken $SU(2)$. The appearance of the Σ_0 breaks the local gauge symmetry $[SU(2) \otimes U(1)]^2$ into its diagonal subgroup $[SU(2) \otimes U(1)]_{SM}$, giving rise to mass of order f for half of the gauge bosons

$$m_{W'} = \frac{f}{2} \sqrt{g_1^2 + g_2^2} = \frac{g}{2sc} f, \quad m_{B'} = \frac{f}{2\sqrt{5}} \sqrt{g_1'^2 + g_2'^2} = \frac{g'}{2\sqrt{5}s'c'} f, \quad (4)$$

with the field rotation to the mass eigenstates given by

$$\begin{aligned} W &= sW_1 + cW_2, & W' &= -cW_1 + sW_2 \\ B &= s'B_1 + c'B_2, & B' &= -c'B_1 + s'B_2. \end{aligned} \quad (5)$$

The mixing angles are given by

$$s = \frac{g_2}{\sqrt{g_1^2 + g_2^2}}, \quad s' = \frac{g_2'}{\sqrt{g_1'^2 + g_2'^2}}. \quad (6)$$

The W and B remain massless and are identified as the SM gauge bosons, with couplings

$$g = g_1 s = g_2 c, \quad g' = g_1' s' = g_2' c'. \quad (7)$$

The couplings of W , W' to two scalars are given by:

$$\begin{aligned} \mathcal{L}_\Sigma(W \cdot W) &= \frac{g^2}{4} \left[W_\mu^a W^{b\mu} - \frac{(c^2 - s^2)}{sc} W_\mu^a W'^{b\mu} \right] \text{Tr} [h^\dagger h \delta^{ab} + 2\phi^\dagger \phi \delta^{ab} + 2\sigma^a \phi^\dagger \sigma^{bT} \phi] \\ &\quad - \frac{g'^2}{4} \left[W_\mu'^a W'^{a\mu} \text{Tr} [h^\dagger h + 2\phi^\dagger \phi] - \frac{(c'^4 + s'^4)}{2s'^2 c'^2} W_\mu'^a W'^{b\mu} \text{Tr} [2\sigma^a \phi^\dagger \sigma^{bT} \phi] \right]. \end{aligned} \quad (8)$$

In the SM, the four-point couplings of the form $WW h^\dagger h$ lead to a quadratically divergent contribution to the Higgs mass. In the littlest Higgs model, however, the $W'W' h^\dagger h$ coupling has an unusual form as seen in Eq. (8), which serves to exactly cancel the quadratic divergence in the Higgs mass arising from the seagull diagram involving a W boson loop. Similarly, the couplings of B , B' to two scalars are:

$$\begin{aligned} \mathcal{L}_\Sigma(B \cdot B) &= g'^2 \left[B_\mu B^\mu - \frac{(c'^2 - s'^2)}{s'c'} B_\mu B'^\mu \right] \text{Tr} \left[\frac{1}{4} h^\dagger h + \phi^\dagger \phi \right] \\ &\quad - g'^2 \left[B'_\mu B'^\mu \text{Tr} \left[\frac{1}{4} h^\dagger h \right] - \frac{(c'^2 - s'^2)^2}{4s'^2 c'^2} B'_\mu B'^\mu \text{Tr} [\phi^\dagger \phi] \right]. \end{aligned} \quad (9)$$

By expanding the nonlinear σ -model field Σ as usual, we obtain the Higgs potential

$$V = \lambda_{\phi^2} f^2 \text{Tr}(\phi^\dagger \phi) + i\lambda_{h\phi h} f (h\phi^\dagger h^T - h^* \phi h^\dagger) - \mu^2 h h^\dagger + \lambda_{h^4} (h h^\dagger)^2, \quad (10)$$

In the littlest Higgs model [24], the naturalness problem induced by the top quark is resolved by introducing a new set of heavy fermions with couplings to the Higgs field such that it cancels the quadratic divergence due to the top quark. The new fermions come in as a vector-like pair, \tilde{t} and \tilde{t}'^c , which are allowed to have a bare mass term which is chosen to be of order f . The coupling of the Standard Model top quark to the pseudo-Goldstone bosons and the heavy vector pair in the littlest Higgs model is chosen to be

$$\mathcal{L}_Y = \frac{1}{2} \lambda_1 f \epsilon_{ijk} \epsilon_{xy} \chi_i \Sigma_{jx} \Sigma_{ky} u_3^c + \lambda_2 f \tilde{t} \tilde{t}'^c + \text{h.c.}, \quad (11)$$

where $\chi_i = (b_3, t_3, \tilde{t})$ and ϵ_{ijk} and ϵ_{xy} are antisymmetric tensors. It is now straightforward to work out the Higgs-heavy quark interactions, as given in Table I, after diagonalizing the mass terms, the physical top quark t and a new heavy quark T can be obtained [24]:

$$\begin{aligned} t_L &= c_L t_3 - s_L \tilde{t}, & t_R^c &= c_R u_3^c - s_R \tilde{t}'^c, \\ T_L &= s_L t_3 + c_L \tilde{t}, & T_R^c &= s_R u_3^c + c_R \tilde{t}'^c, \end{aligned}$$

As a summary, the couplings, related to our calculation, of the new particles to the SM particles, which include 1) the three-point couplings of the gauge boson to the scalars, including case I, one gauge boson to two scalars and case II, two gauge bosons and one scalar, 2) charged gauge boson-fermion couplings, 3) the scalar-fermion couplings, can be approximately written here as [24]:

particles	vertices	particles	vertices
$W_{L\mu}^+ H \Phi^-$	$-\frac{ig}{2} (\sqrt{2}s_0 - s_+) (p_1 - p_2)_\mu$	$W_{L\mu}^+ A_{H\nu} \Phi^-$	$-\frac{i}{2} gg' \frac{(c'^2 - s'^2)}{2s'c'} (vs_+ - 4v') g_{\mu\nu}$
$W_{L\mu}^+ \Phi^0 \Phi^-$	$-\frac{ig}{\sqrt{2}} (p_1 - p_2)_\mu$	$W_{L\mu}^+ Z_{L\nu} \Phi^-$	$-i \frac{g^2}{c_w} v' g_{\mu\nu}$
$W_{L\mu}^+ \Phi^P \Phi^-$	$\frac{g}{\sqrt{2}} (p_1 - p_2)_\mu$	$W_{L\mu}^+ Z_{H\nu} \Phi^-$	$ig^2 \frac{(c^2 - s^2)}{2sc} v' g_{\mu\nu}$
$W_L^{+\mu} \bar{t}_L b_L$	$\frac{ig}{\sqrt{2}} \left[1 - \frac{v^2}{f^2} \left(\frac{1}{2} x_L^2 + \frac{1}{2} c^2 (c^2 - s^2) \right) \right] \gamma^\mu V_{tb}^{SM}$	$W_L^{+\mu} \bar{T}_L b_L$	$\frac{g}{\sqrt{2}} \frac{v}{f} x_L \gamma^\mu V_{tb}^{SM}$
$H \bar{t} t$	$-i \frac{m_t}{v} \left[1 - \frac{1}{2} s_0^2 + \frac{v}{f} \frac{s_0}{\sqrt{2}} - \frac{2v^2}{3f^2} + \frac{v^2}{f^2} \frac{\lambda_1^2}{\lambda_1^2 + \lambda_2^2} \left(1 + \frac{\lambda_1^2}{\lambda_1^2 + \lambda_2^2} \right) \right]$	$H \bar{T} T$	$-i \frac{\lambda_1^2}{\sqrt{\lambda_1^2 + \lambda_2^2}} \left(1 + \frac{\lambda_1^2}{\lambda_1^2 + \lambda_2^2} \right) \frac{v}{f}$
$\Phi^0 \bar{t} t$	$-\frac{im_t}{\sqrt{2}v} \left(\frac{v}{f} - \sqrt{2}s_0 \right)$	$\Phi^P \bar{t} t$	$-\frac{m_t}{\sqrt{2}v} \left(\frac{v}{f} - \sqrt{2}s_P \right) \gamma^5$
$\Phi^+ \bar{t} b$	$-\frac{i}{\sqrt{2}v} (m_t P_L + m_b P_R) \left(\frac{v}{f} - 2s_+ \right)$	$\Phi^+ \bar{T} b$	$-\frac{im_t}{\sqrt{2}v} \left(\frac{v}{f} - 2s_+ \right) \frac{\lambda_1}{\lambda_2} P_L$

TABLE I: the three-point couplings of the gauge boson to the scalars, the charged gauge boson-fermion couplings and the scalar-fermion couplings in the lightest higgs models. The momenta are assigned according to $V_\mu S_1(p_1) S_2(p_2)$. All particles are the mass eigenstates and all momenta are out-going.

Of which, the charged gauge boson-fermion couplings are purely left-handed, and the projection operator $P_L = (1 - \gamma^5)/2$ is implied. We define $x_L \equiv \lambda_1^2/(\lambda_1^2 + \lambda_2^2)$ to shorten the notation, where λ_1, λ_2 are the Yukawa coupling of order $\mathcal{O}(1)$.

The neutral gauge boson-fermion couplings can also be written as those in Table II [24]. The anomaly cancellation requires $y_u = -2/5$ and $y_e = 3/5$ and the couplings are in the form $i\gamma^\mu (g_V + g_A \gamma^5)$.

particles	g_V	g_A
$Z_L \bar{u} u$	$-\frac{g}{2c_w} \left\{ \left(\frac{1}{2} - \frac{4}{3} s_w^2 \right) - \frac{v^2}{f^2} \left[c_w x_Z^{W'} c/2s + \frac{s_w x_Z^{B'}}{s'c'} \left(2y_u + \frac{7}{15} - \frac{1}{6} c'^2 \right) \right] \right\}$	$-\frac{g}{2c_w} \left\{ -\frac{1}{2} - \frac{v^2}{f^2} \left[-c_w x_Z^{W'} c/2s + \frac{s_w x_Z^{B'}}{s'c'} \left(\frac{1}{5} - \frac{1}{2} c'^2 \right) \right] \right\}$
$Z_L \bar{d} d$	$-\frac{g}{2c_w} \left\{ \left(-\frac{1}{2} + \frac{2}{3} s_w^2 \right) - \frac{v^2}{f^2} \left[-c_w x_Z^{W'} c/2s + \frac{s_w x_Z^{B'}}{s'c'} \left(2y_u + \frac{11}{15} + \frac{1}{6} c'^2 \right) \right] \right\}$	$-\frac{g}{2c_w} \left\{ \frac{1}{2} - \frac{v^2}{f^2} \left[c_w x_Z^{W'} c/2s + \frac{s_w x_Z^{B'}}{s'c'} \left(-\frac{1}{5} + \frac{1}{2} c'^2 \right) \right] \right\}$
$A_H \bar{u} u$	$\frac{g'}{2s'c'} \left(2y_u + \frac{17}{15} - \frac{5}{6} c'^2 \right)$	$\frac{g'}{2s'c'} \left(\frac{1}{5} - \frac{1}{2} c'^2 \right)$
$A_H \bar{d} d$	$\frac{g'}{2s'c'} \left(2y_u + \frac{11}{15} + \frac{1}{6} c'^2 \right)$	$\frac{g'}{2s'c'} \left(-\frac{1}{5} + \frac{1}{2} c'^2 \right)$
$Z_H \bar{u} u$	$gc/4s$	$-gc/4s$
$Z_H \bar{d} d$	$-gc/4s$	$gc/4s$

TABLE II: Neutral gauge boson-fermion couplings and anomaly cancellation requires $y_u = -2/5$ and $y_e = 3/5$. We write the couplings in the form $i\gamma^\mu (g_V + g_A \gamma^5)$.

B. the $LH \phi W$ associated production at the LHC

At the LHC, the parton level cross sections are calculated at the leading order as

$$\hat{\sigma}(\hat{s}) = \int_{\hat{t}_{min}}^{\hat{t}_{max}} \frac{1}{16\pi\hat{s}^2} \overline{\Sigma} |M_{ren}|^2 d\hat{t}, \quad (12)$$

with

$$\hat{t}_{max,min} = \frac{1}{2} \left\{ m_{p_1}^2 + m_{p_2}^2 - \hat{s} \pm \sqrt{[\hat{s} - (m_{p_1} + m_{p_2})^2][\hat{s} - (m_{p_1} - m_{p_2})^2]} \right\}, \quad (13)$$

where p_1 and p_2 are the first and the second initial particles in the parton level, respectively. For our case, they could be gluon g and quarks u, d, c, s, b etc.

The total hadronic cross section for $pp \rightarrow SS' + X$ can be obtained by folding the subprocess cross section $\hat{\sigma}$ with the parton luminosity

$$\sigma(s) = \int_{\tau_0}^1 d\tau \frac{dL}{d\tau} \hat{\sigma}(\hat{s} = s\tau), \quad (14)$$

where $\tau_0 = (m_{p_1} + m_{p_2})^2/s$, and s is the pp center-of-mass energy squared. $dL/d\tau$ is the parton luminosity given by

$$\frac{dL}{d\tau} = \int_x^1 \frac{dx}{x} [f_{p_1}^p(x, Q) f_{p_2}^p(\tau/x, Q) + (p_1 \leftrightarrow p_2)], \quad (15)$$

where $f_{p_1}^p$ and $f_{p_2}^p$ are the parton p_1 and p_2 distribution functions in a proton, respectively. In our numerical calculation, the CT6L1 parton distribution function is used [25] and take factorization scale Q and the renormalization scale μ_F as $Q = \mu_F = m_\phi + m_W$. The loop integrals are evaluated by the LoopTools package [26].

As for the SM parameters, throughout this paper, we take $m_t = 173$ GeV [27], $m_W = 80.38$ GeV, $m_Z = 91.19$ GeV, and $G_F = 1.16637 \times 10^{-5} \text{GeV}^{-2}$ [28], $\alpha_s(m_Z) = 0.118$ and neglect bottom quark mass as well as other light quark masses.

Now we discuss the main involved LH parameters,

- (1) new scalar masses, which include the charged pseudo boson, neutral bosons and the SM higgs. We here choose the SM-like higgs mass as the current Experiment value: 125 GeV [1, 2] and the masses of others, despite of the small electromagnetic difference, are the same, m_ϕ , as a free parameter varying from 200 GeV to 600 GeV.
- (2) The mixing parameter s , c and s' , c' , which are in the range of $0 \sim 1$. We will here take, however, s free parameter from $0 - 0.5$, and take $s' = 0.5$ so as the $c' > 0.62$ according to Ref. [29].
- (3) As for the scale f , for light higgs mass, we have [24]

$$m_H^2 = 2\mu^2 \simeq a_{1\text{-loop}} \frac{f^2}{16\pi^2} + a_{2\text{-loop}} \frac{f^2}{16\pi^2}, \quad (16)$$

with both $a_{1\text{-loop}}$ (we have absorbed a factor of $\log(16\pi^2)$ into the definition of $a_{1\text{-loop}}$) and $a_{2\text{-loop}}$ containing many contributions (terms) from different interactions. Assuming that there is no large cancellation and m_H^2 is no less than 10% of the magnitude of the largest term on the right-hand side of Eq. (16), a rough estimate of the natural scale is obtained [24]

$$f \leq \frac{4\pi m_H}{\sqrt{0.1 a_{\max}}} \simeq \frac{8 \text{ TeV}}{\sqrt{a_{\max}}} \left(\frac{m_H}{200 \text{ GeV}} \right), \quad (17)$$

where a_{\max} denotes the largest coefficient of the terms in Eq. (16) which could be of the order of 10. So $f < 1.6$ TeV, we here take $500 < f < 2000$ GeV.

- (4) About the new gauge boson masses, the final mass eigenstates for the charged gauge bosons are W_L (light) and W_H (heavy), with masses to the order of v^2/f^2 given by [24]

$$M_{W_L^\pm}^2 = m_w^2 \left[1 - \frac{v^2}{f^2} \left(\frac{1}{6} + \frac{1}{4}(c^2 - s^2)^2 \right) + 4 \frac{v'^2}{v^2} \right], \quad (18)$$

$$M_{W_H^\pm}^2 = m_w^2 \left(\frac{f^2}{s^2 c^2 v^2} - 1 \right), \quad (19)$$

The neutral gauge boson masses are similarly given by

$$M_{A_L}^2 = 0, \quad (20)$$

$$M_{Z_L}^2 = m_z^2 \left[1 - \frac{v^2}{f^2} \left(\frac{1}{6} + \frac{1}{4}(c^2 - s^2)^2 + \frac{5}{4}(c'^2 - s'^2)^2 \right) + 8 \frac{v'^2}{v^2} \right], \quad (20)$$

$$M_{A_H}^2 = m_z^2 s_w^2 \left(\frac{f^2}{5s'^2 c'^2 v^2} - 1 + \frac{x_H c_w^2}{4s^2 c^2 s_w^2} \right) \quad (21)$$

$$M_{Z_H}^2 = m_w^2 \left(\frac{f^2}{s^2 c^2 v^2} - 1 - \frac{x_H s_w^2}{s'^2 c'^2 c_w^2} \right), \quad (22)$$

where $m_z \equiv gv/(2c_w)$ is the SM limit when $f \rightarrow \infty$ and the x_H is given in Ref. [24],

$$x_H = \frac{5}{2}gg' \frac{s c s' c' (c^2 s'^2 + s^2 c'^2)}{(5g^2 s'^2 c'^2 - g'^2 s^2 c^2)}. \quad (23)$$

- (5) If we define $x = 4fv'/v^2$, which parameterizes the vev of the scalar of the triplet ϕ . So the mass of the neutral scalar boson in Eq.22 can be rewritten as [24, 30]

$$\begin{aligned} M_{W_L}^2 &= (m_W)^2 \left\{ 1 - \frac{v^2}{f^2} \left[\frac{1}{6} + \frac{1}{4}(c^2 - s^2)^2 + \frac{x^2}{4} \right] \right\}, \\ M_{\phi^0}^2 &= \frac{2m_{H^0}^2 f^2}{v^2 [1 - (4v'f/v^2)^2]} = \frac{2m_{H^0}^2 f^2}{v^2 (1 - x^2)} \end{aligned} \quad (24)$$

The above equation about the mass of ϕ^0 requires a constraint of $0 \leq x < 1$ (i.e., $4v'f/v^2 < 1$), which shows the relation between the scale f and the vev of the higgs field doublets and the triplet (v, v'). We can also take x as a free parameter ($0 < x < 1$).

- (6) Finally, note that the W_L mass gets a correction at order v^2/f^2 , which will modify the relation among the W mass, g , and G_F . In the LH model, the relation among the Fermi coupling constant G_F , the gauge boson W mass M_W and the fine structure constant α can be written as[31]:

$$\frac{G_F}{\sqrt{2}} = \frac{\pi\alpha}{2M_W^2 s_W^2} \left[1 - c^2(c^2 - s^2) \frac{v^2}{f^2} + 2c^4 \frac{v^2}{f^2} - \frac{5}{4}(c'^2 - s'^2) \frac{v^2}{f^2} \right] \quad (25)$$

So we have

$$\frac{e^2}{s_W^2} = \frac{4\sqrt{2}G_F M_W^2}{[1 - c^2(c^2 - s^2) \frac{v^2}{f^2} + 2c^4 \frac{v^2}{f^2} - \frac{5}{4}(c'^2 - s'^2) \frac{v^2}{f^2}]} \quad (26)$$

C. numerical results in littlest higgs model

Due to the interactions in Tables I and II, the single charged boson production associated with the W boson processes can proceed through various parton processes at the LHC, as shown in Fig.1, in which those obtained by exchanging the two external gluon lines are not displayed here. To know the relative values of them, we here, firstly, discuss the contributions from every single parton channel though , actually, we can not distinguish the initial states, i.e, we will firstly discuss the gg fusion and the $q\bar{q}$ annihilation processes, respectively, and then sum them all together to see the total contributions.

1. gg fusion in the LH models

Note that the processes consist of the box diagrams and the W scalar scalar coupling, just shown as Fig. 1(a) and (b)(c), The s-channel contribution of the cross sections, however, is tiny, which is easy to understand with the quite large center-of-mass depression.

The production cross sections of the ϕ^+W^- of the gg fusion are plotted in Figs. 2 for $\sqrt{S} = 8, 14$ TeV, respectively, with $x = 0.1, 0.3, 0.5, 0.7$ and $f = 500$ GeV, as functions of the scalar mass m_ϕ , assuming the charged and neutral scalar mass degenerate, $m_{\phi^\pm} = m_{\phi^0} = m_{\phi^p}$. From Figs. 2, we can see the cross section of this process is quite large, about 100 fb in most of the parameter space and, as was expected, the production rate decreases with the increasing scalar mass since the phase space are depressed by the mass.

To compare the other parameter dependence, in figs. 3 we give the cross sections depend on the parameter f and s , for $\sqrt{S} = 8, 14$ TeV, $f = 500$ GeV, and $m_\phi = 200$ GeV, which can clearly show the production rate varying as the different parameter. We can see the increasing production rate with the increasing s , but the cross section is decreasing when f grows up.

In Figs. 2, 3 we can also see the x dependence of the process $gg \rightarrow \phi^+W^-$ is very strong since the x ($= 4fv'/v^2$) is closely connected to the triplet vev v' , and the v' decide the mixing parameter s_+ , the parameter involved in the $\phi^+ \bar{t}(T)b$. The production cross sections of the processes $gg \rightarrow W^+\phi^- + X$ decrease with the increasing parameter x . For example, when the center-of-mass is 8 TeV, for $x = 0.1$, $m_\phi = 200$ GeV, and $s = 0.1$, the production rate is

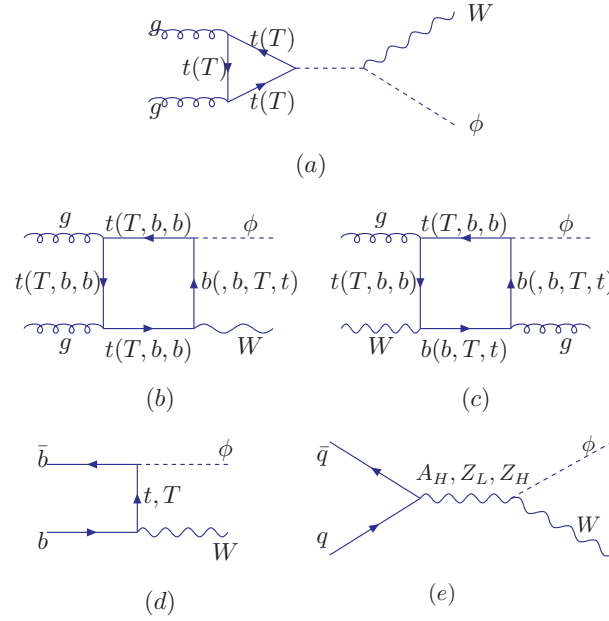


FIG. 1: Feynman diagrams for the charged scalar production associated with the W boson at the LHC via gluon fusion and the quark anti-quark annihilation parton level processes in the LH model. Those obtained by exchanging the two external gluon lines are not displayed here.

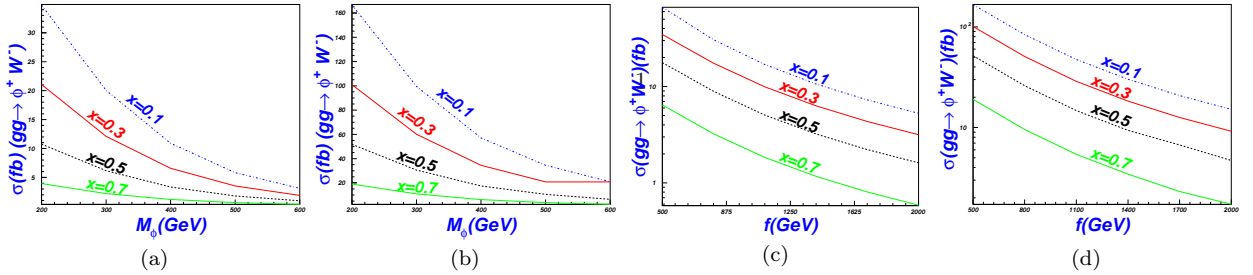


FIG. 2: In LH, the cross section σ of the processes $gg \rightarrow \phi^+ W^-$ as a function of the scalar mass m_ϕ with $\sqrt{S} = 8$ TeV (a) and $\sqrt{S} = 14$ TeV (b) respectively, for $f = 500$ GeV and $s = 0.1$, with different x $x = 0.1, 0.3, 0.5, 0.7$; the cross section σ of the processes $gg \rightarrow \phi^+ W^-$ as a function of f with $\sqrt{S} = 8$ TeV (c) and $\sqrt{S} = 14$ TeV (d) respectively, and $s = 0.1$, with different x ($x = 0.1, 0.3, 0.5, 0.7$);

about 66 fb; When $x = 0.3$, however, the production rate declines to only 34 fb. The larger the x is, the smaller the cross section is. When the center-of-mass is 14 TeV, the same situation occurs, just the rate will be about an order larger than those of the smaller center-of-mass, i.e. 8 TeV.

The mixing s affects the process $gg \rightarrow \phi^+ W^-$ largely, too, however, the trend is different. We can see from Fig. 3 (c) that the possibility of the $\phi^+ W^-$ associated production increases with increasing s . In Figs. 2, 3(a)(b), we take $s = 0.1$, which is quite small compared to its maximum value, 0.5, according to the discussion of Ref. [29]. So our discussion are not the maximum, the results are general.

The parameter $x = 0.1$ in Figs. 2, for the t-channel production dominant processes, including the $b\bar{b} \rightarrow \phi^+ W^-$, is a little large value for the cross section, since the t-channel productions decrease with the increasing x , which will be seen clearly in Figs. 5(a)(b) and Fig.7.

Similarly, we can see from Fig. 2(c)(d) that the process $gg \rightarrow \phi^+ W^-$ is dependent strongly on the parameter f , which is understandable since, the most couplings in the LH models, such as $\phi^+ t(T)b$ and $\phi^+ W^- S$ ($S = \phi^0, \phi^p, H$), etc, are tightly connected with the parameter f . The cross sections may be large if the scale f is not too high and decreases rapidly as the increasing f . The rates of the $\phi^+ W^-$ production for $\sqrt{s} = 14$ TeV, for example, can arrive at about 273 fb, 35 fb and 24 fb, for $f = 500, 1000$ and 2000 GeV, respectively, with $s = 0.1$.

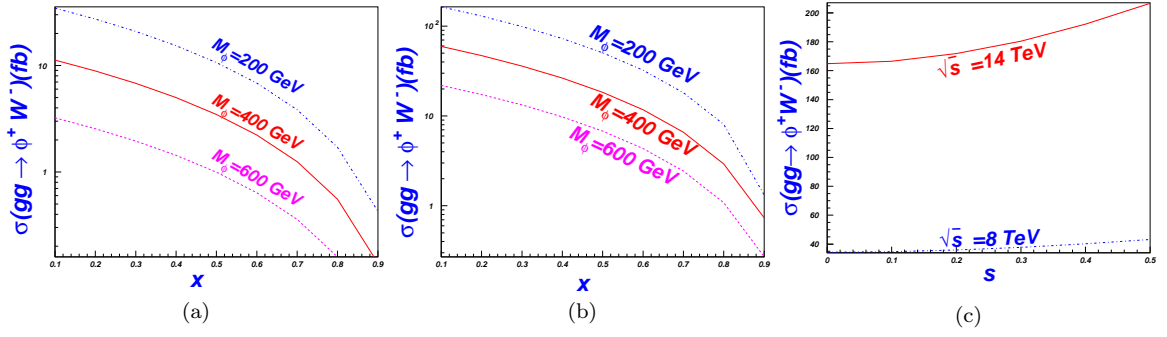


FIG. 3: In LH, when the scalar mass $m_\phi = 200, 400, 600$ GeV, the cross section σ of the processes $gg \rightarrow \phi^+ W^-$ as a function of x with $\sqrt{S} = 8$ TeV (a) and $\sqrt{S} = 14$ TeV (b) respectively, and $s = 0.1$, with $f = 500$ GeV; The cross section σ of the processes $gg \rightarrow \phi^+ W^-$ as a function of s for $x = 0.1$, $f = 500$ GeV and $\sqrt{S} = 8$ TeV and $\sqrt{S} = 14$ TeV (c).

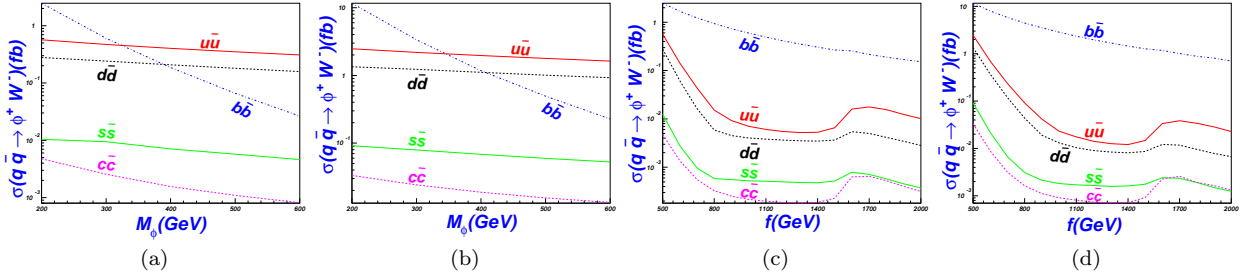


FIG. 4: In LH, the cross section σ of the processes $q\bar{q} \rightarrow \phi^+ W^-$ as a function of the scalar mass m_ϕ with $\sqrt{S} = 8$ TeV (a) and $\sqrt{S} = 14$ TeV (b) for $f = 500$ GeV, $x = 0.1$ and $s = 0.1$, here $q = u, d, c, s, b$ quarks.

2. ϕW production via quark anti-quark annihilation

In LH, the ϕW production via quark anti-quark annihilation are realized by the parton level $u\bar{u}$, $d\bar{d}$, $c\bar{c}$, $s\bar{s}$, $b\bar{b} \rightarrow \phi W$, which can be distinguished as t-channel and s-channel processes, but the t-channel are only realized by the $b\bar{b}$ initial state, via $\phi^+ \bar{t}(T)b$ couplings.

And for the s-channel scalar and W boson associated production induced by the $q\bar{q}$ ($q = u, d, s, c, b$) collision, what makes the difference among them is only, if we neglect the masses of the quarks u, d, c, s, b , the parton distribution function in the proton, so it is naturally to see in Fig.4 that $\sigma(u\bar{u}) > \sigma(d\bar{d}) > \sigma(s\bar{s}) > \sigma(c\bar{c}) > \sigma(b\bar{b})$.

In Figs. 4(a)(b), we can see the cross sections decrease with increasing charged scalar mass m_ϕ , the level of decline, however, is different. For $b\bar{b}$ realization, we can see it declines rapidly, while the $u\bar{u}$, $d\bar{d}$, $s\bar{s}$, $c\bar{c}$ annihilations are not so quickly. That can be understood that with the small distribution in the proton, the $b\bar{b}$ collisions mainly contribute via the t-channel, while the others are from s-channels mediated by the bosons A_H , Z_L , Z_H which appear in the propagator, with large masses about 1 TeV, which weakens the effect of the increasing scalar mass. When m_ϕ is not too large compared to the heavy boson mass, the cross sections from s-channel $q\bar{q}$ annihilations are almost unchanged. Actually, if we assume the ϕ^+ mass are in the order of the heavy bosons, i.e, more than 1 TeV, the situation is different immediately. With the increasing m_ϕ , the production rates decrease largely, which is verified by our calculation though not shown here.

The s-channel processes in Fig. 1 (e), though the parton distribution functions are larger for the $u\bar{u}$ and $d\bar{d}$ initial states, may be relatively small in view of the center-of-mass depression effects. At the same time, the t-channel coupling strengths may be large for little x . In Fig. 1(d), For instance, the strengthen of $\phi^+ \bar{t}(T)b \sim m_t/v \sim 1$ contributes large. so no wonder the cross sections of the parton level processes like $u\bar{u}(d\bar{d}, s\bar{s}) \rightarrow \phi W$ are smaller than those of the others even with larger parton distribution functions, especially with the increasing f . These can be seen clearly in Figs. 4(c)(d).

Note that in Fig.4 the processes depend largely on the parameter f , and if the parameter f decreases, the production rate of this process will go up rapidly. From the couplings, this can also be see clearly that the $\phi \bar{T}(t) \sim 1/f$, while in the s-channel, the couplings $V\phi W$ ($V = A_H, Z_L, Z_H$) $\sim v'$, $v' = xv^2/(4f)$, so they decrease with increasing f . The exception, however, occur in Fig. 4(c)(d) and therefore Fig. 5.

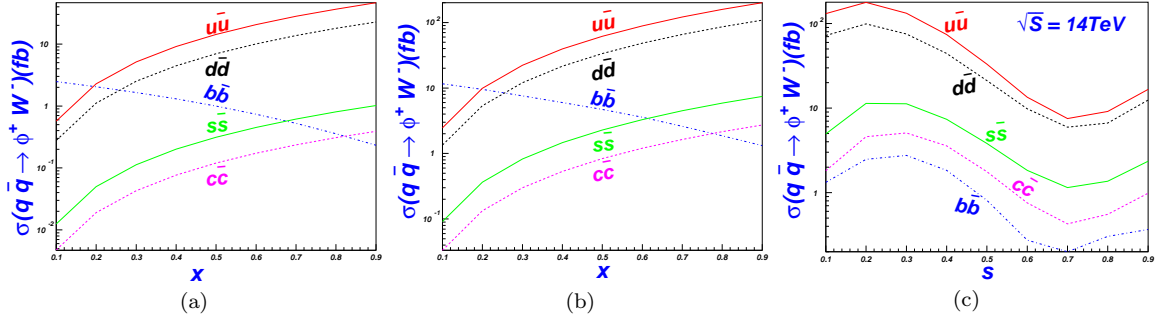


FIG. 5: In LH, the cross section σ of the processes $q\bar{q} \rightarrow \phi^+ W^-$, with $m_\phi = 200$ GeV, $f = 500$ GeV as a function of x and s for $\sqrt{S} = 8$ TeV (a), for $\sqrt{S} = 14$ TeV ($s = 0.1$) and $\sqrt{S} = 14$ TeV ($x = 0.9$).

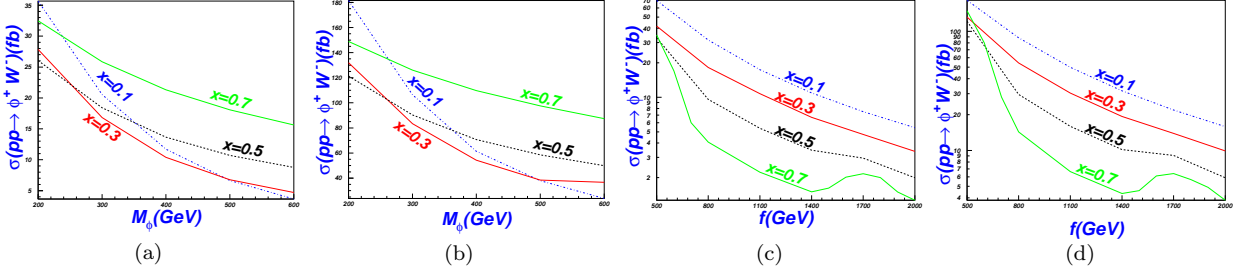


FIG. 6: In LH models, the total cross section σ of the processes $pp \rightarrow \phi^+ W^-$ as a function of the scalar mass m_ϕ with $\sqrt{S} = 8$ TeV (a) and $\sqrt{S} = 14$ TeV (b) for $s = 0.1$, $f = 500$ GeV and $x = 0.1, 0.3, 0.5, 0.7$; The total cross section σ of the processes $pp \rightarrow \phi^+ W^-$ as a function of f with the scalar mass $m_\phi = 200$ GeV, $s = 0.1$ and $\sqrt{S} = 8$ TeV (c) and $\sqrt{S} = 14$ TeV (d) for $x = 0.1, 0.3, 0.5, 0.7$.

From Fig. 4, we can also see that, when x is small, such as 0.1 which we have chosen, in the most parameter space, the largest channel of the processes $q\bar{q} \rightarrow \phi W$ is the $b\bar{b} \rightarrow \phi W$, which is easy to understand since, in Fig.1, the t-channel process (d) is free of the center-of-mass depression and the upraise via x i.e, the v' does not reveal itself. For larger x , however, the situation changes. we can see from Fig.5 that, except via $b\bar{b}$ annihilation, the quark anti-quark processes are increasing with the increasing x .

But, in Fig. 5, we can see that with the increasing parameter $x = 4fv'/v^2$, it is totally different. When $x > 0.2$ the cross sections from the $u\bar{u}$ collision begin overwhelming that from $b\bar{b}$ at 14 TeV, which is opposite to the above discussion. The reason is given in the following, the same as the comparison of ϕW production via gg fusion and $q\bar{q}$ annihilation.

Now, compared the Fig. 3(c) with Figs. 5, 7, we can find that the ϕW associated production from gg fusion and $b\bar{b}$ annihilation decreases with increasing x , while those from other quark anti-quark annihilation ($u\bar{u}$, $d\bar{d}$, $s\bar{s}$ and $c\bar{c}$) is opposite, which is understandable from their different coupling forms. Since the $VW_L\phi^+$ ($V = A_L, Z_L, Z_H$) is proportional to v' , while $\phi\bar{l}(T)b$ is in proportion to $\frac{v}{f} - 2s_+$, here $s_+ = 2v'/v$. In the scalar-fermion couplings, actually, there is a competition between the two terms $\frac{v}{f}$ and $2s_+$. When $f = 500$ GeV, $v/f \sim 0.5$, the $2s_+$, however, less than 0.5 all the time if we satisfy the requirement $v' < 30$, i.e, $x < 1$ [24], so with the increasing v' , the couplings $\phi\bar{l}(T)b$ is decreasing.

In Fig. 5(c) we also show the s parameter dependence of the cross sections from the quark anti-quark annihilation, we can see from which that the s -dependence of the ϕW production via $q\bar{q}$ annihilation is not straight, due to the couplings of $Vq\bar{q}$ and $V\phi W$ ($V = Z_L, Z_H, A_H$), so it is not strange that in some little area, the cross sections are quite large.

3. Total contribution of the gg and quark anti-quark annihilation

In Figs. 6,7 we sum the contributions from all the parton level processes. We can see from the figures that the cross sections can arrive at tens of fb even when $\sqrt{S} = 8$ TeV, and when the center-of-mass rises to 14 TeV, the production

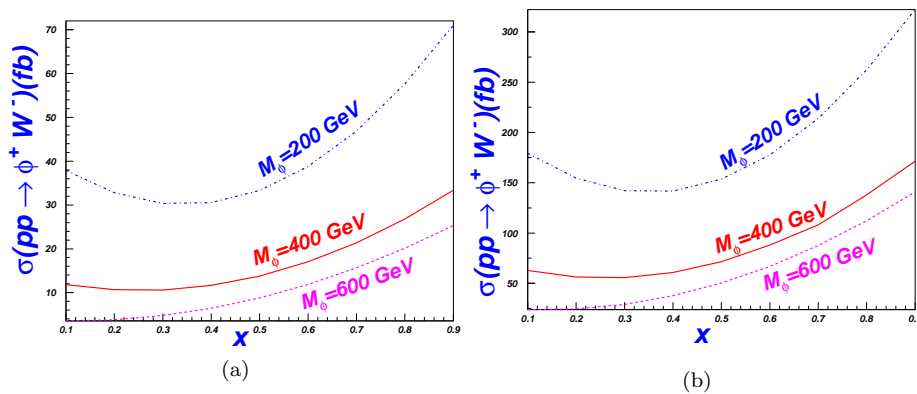


FIG. 7: The total cross section σ of the processes $pp \rightarrow \phi^+ W^-$ as a function of x with the scalar mass $m_\phi = 200, 400, 600$ GeV, $s = 0.1$ and $\sqrt{S} = 8$ TeV(a) and $\sqrt{S} = 14$ TeV(b).

rates will become more large, larger than 100 fb in quite a large parameter space. So in the discussion of reducing the backgrounds, we will concentrate to the 14 TeV center of mass.

with the increasing x , the s-channel contributions of the $q\bar{q}$ annihilation contribute more and more large, so then the gg fusion and $b\bar{b}$ collision, the t-channel dominant, are not the largest any more, but instead, the uu and dd will control the situation, which can be seen clearly in Fig.6.

From Figs. 6 we can see that the production rates of the $\phi^+ W^-$ decrease when m_ϕ or f goes up. Note that in Fig.6 (c)(d), with the increasing f , in the tail of the curve for $pp \rightarrow \phi^+ W^-$, $x = 0.7$, the cross sections increase when f changes from 1500 GeV to 1700 GeV, which is understandable, when x is large, the contributions from the s-channel surpass that from the t-channel, i.e, the gg and $b\bar{b}$ realization.

III. THE LRTH MODEL AND ϕW PRODUCTION AT THE LHC

A. The LRTH model and the relevant couplings

The left right twin Higgs mechanism has been proposed as a solution to the little hierarchy problem [32, 33]. The Higgses emerge as pseudo-Goldstone bosons once the global symmetry is spontaneously broken. Gauge and Yukawa interactions that break the global symmetry give masses to the Higgses, with the leading order being quadratically divergent. When an additional discrete symmetry is imposed, the leading quadratically divergent terms respect the global symmetry. Thus they do not contribute to the Higgs masses. The resulting Higgs masses obtain logarithmically divergent contributions. The Higgs masses are around the electroweak scale when the cutoff is around 5 – 10 TeV.

The twin Higgs mechanism can be implemented in left-right models with the discrete symmetry being identified with left-right symmetry [32]. In the left-right twin Higgs (LRTH) model, the global symmetry is $U(4) \times U(4)$, with a gauged $SU(2)_L \times SU(2)_R \times U(1)_{B-L}$ subgroup. After Higgses obtain vacuum expectation values, the global symmetry $U(4) \times U(4)$ breaks down to $U(3) \times U(3)$, and $SU(2)_R \times U(1)_{B-L}$ breaks down to the SM $U(1)_Y$. Three Goldstone bosons are eaten by the massive gauge bosons Z_H and W_H^\pm , while the remaining Goldstone bosons contain the SM $SU(2)_L$ Higgs doublet and extra Higgses. The leading quadratically divergent SM gauge boson contributions to the Higgs masses are canceled by the loop involving the heavy gauge bosons. A vector top singlet pair is introduced to generate an $\mathcal{O}(1)$ top Yukawa coupling. The quadratically divergent SM top contributions to the Higgs potential are canceled by the contributions from a heavy top partner. Many new particles which have order of one interaction strength with the SM sector are predicted and rich phenomenology is expected at the LHC.

Two Higgs fields, H and \hat{H} , are introduced and each acquires a non-zero vev which breaks one of the $U(4)$ to $U(3)$ and yields 14 Goldstone bosons. Six out of the fourteen Goldstone bosons are eaten by the massive gauge bosons. After the re-parametrization of the fields, we are left with one neutral pseudoscalar ϕ^0 , a pair of charged scalar ϕ^\pm , the SM physical Higgs h , and a $SU(2)_L$ doublet $\hat{h} = (\hat{h}_1^+, \hat{h}_2^0)$.

The Higgs vevs also break $SU(2)_R \times U(1)_{B-L}$ down to the SM $U(1)_Y$ and generates four charged and two neutral gauge bosons : W^\pm , W_H^\pm , Z and Z_H . W and Z are the usual massive gauge bosons in the SM and W_H , and Z_H are three additional massive gauge bosons with masses of a few TeV.

The Lagrangian concerning of the new particles can be written as

$$\mathcal{L} = \mathcal{L}_H + \mathcal{L}_G + \mathcal{L}_f + \mathcal{L}_Y + \mathcal{L}_{one-loop} + \mathcal{L}_\mu. \quad (27)$$

The various pieces in Eq. (27), in the order in which they are written, are covariant kinetic terms for Higgses, gauge bosons and fermions, Yukawa interactions, one-loop Coleman-Weinberg (CW) potential [34] for Higgses and soft symmetry breaking μ terms.

Once H and \hat{H} obtain vevs, the Higgs kinetic term \mathcal{L}_H gives rise to the gauge boson mass terms. When H and \hat{H} get vevs $SU(2)_L \times SU(2)_R \times U(1)_{B-L}$ breaks down to $U(1)_{EM}$. There are six massive gauge bosons W^\pm , W_H^\pm , Z , Z_H , and one massless photon γ . For the charged gauge bosons, there is no mixing between the W_L^\pm and the W_R^\pm : $W^\pm = W_L^\pm$ and $W_H^\pm = W_R^\pm$.

Using the appropriate nonlinear Higgs representation and the unitary gauge choice given in Ref. [33], we obtain the derivative self-interactions of the scalars and the interactions between scalars and gauge bosons. The kinetic term for the gauge bosons, \mathcal{L}_G , is standard. It gives us three and four gauge boson self-couplings. The covariant kinetic term for fermions, \mathcal{L}_f , is straight forward to write down once the gauge representations of all fermions are known. It gives rise to the gauge interactions of fermions. The Yukawa coupling \mathcal{L}_Y couples fermions to Higgses. It generates the fermion masses once Higgses get vevs. It also gives rise to scalar-fermion-fermion Yukawa interactions. $U(4)$ violating interactions, i.e. the gauge couplings and Yukawa couplings, generate a potential for the Goldstone bosons at loop level, which is indicated by $\mathcal{L}_{one-loop}$ for the one-loop contribution. In particular, it generates mass terms for the Goldstone Higgses. The neutral scalar ϕ^0 , however, remains massless due to a residual $U(1)$ global symmetry. A ‘ μ -term’ is introduced to break the global $U(1)$ symmetry softly in order to give a mass to ϕ^0 . This μ -term inevitably gives masses to other scalars. Other μ -terms could be added to generate masses for other Higgses, for example, the dark matter candidate \hat{h}_2^0 .

Summarily, the kinetic terms of higgs, the gauge bosons, \mathcal{L}_G , fermions, \mathcal{L}_f , the Yukawa coupling \mathcal{L}_Y of fermions to Higgses, the one-loop CW potential [34] the μ -term can written as

$$\mathcal{L}_H = (D_\mu H)^\dagger D^\mu H + (D_\mu \hat{H})^\dagger D^\mu \hat{H}, \quad (28)$$

$$\mathcal{L}_G = -\frac{1}{2}\text{tr}(F_{\mu\nu})_L(F^{\mu\nu})_L - \frac{1}{2}\text{tr}(F_{\mu\nu})_R(F^{\mu\nu})_R - \frac{1}{4}\text{tr}(F_{\mu\nu})_{B-L}(F^{\mu\nu})_{B-L}, \quad (29)$$

$$\begin{aligned} \mathcal{L}_f &= \bar{L}_\alpha i\gamma_\mu(\partial^\mu - ig_2 W_2^\mu + ig_1 W_{B-L}^\mu)L_\alpha + \bar{Q}_\alpha i\gamma_\mu(\partial^\mu - ig_2 W_2^\mu - i\frac{g_1}{3}W_{B-L}^\mu)Q_\alpha \\ &+ \bar{q}i\gamma_\mu(\partial^\mu - i\frac{4g_1}{3}W_{B-L}^\mu)q \end{aligned} \quad (30)$$

$$\begin{aligned} \mathcal{L}_Y &= \frac{y_u^{\alpha\beta}}{\Lambda}(\bar{Q}_{L\alpha}\tau_2 H_L^*)(H_R^T\tau_2 Q_{R\beta}) + \frac{y_d^{\alpha\beta}}{\Lambda}(\bar{Q}_{L\alpha}H_L)(H_R^\dagger Q_{R\beta}) \\ &+ y_L\bar{Q}_{L3}\tau_2 H_L^* q_R + y_R\bar{Q}_{R3}\tau_2 H_R^* q_L - M\bar{q}_L q_R + h.c. \end{aligned} \quad (31)$$

$$V_{CW} = \sum_i \frac{1}{64\pi^2} M_i^4 (\ln \frac{M_i^2}{\Lambda^2} + \alpha), \quad (32)$$

$$V_\mu = -\mu_l^2(H_L^\dagger \hat{H}_L + h.c.) - \mu_r^2(H_R^\dagger \hat{H}_R + h.c.) + \hat{\mu}^2 \hat{H}_L^\dagger \hat{H}_L. \quad (33)$$

In the equations above, the covariant derivative $D^\mu = \partial^\mu - ig_2 W_2^\mu - ig_1 n_{B-L} W_{B-L}^\mu$; g_1 and g_2 are the gauge couplings for $U(1)_{B-L}$ and $SU(2)_{L,R}$, and n_{B-L} is the charge of the field under $U(1)_{B-L}$. $(F_{\mu\nu})_{L,R}$ and $(F_{\mu\nu})_{B-L}$ are the field strength for $SU(2)_{L,R}$ and $U(1)_{B-L}$, respectively. ‘ α ’, ‘ β ’ is the family index which runs from 1 to 3 and under left-right symmetry, $y_L = y_R = y$.

In the Yukawa coupling \mathcal{L}_Y , a non-zero value of M leads to the mixing between the SM-like top quark and the heavy top quark. The larger the value of M , the larger the mixing between the two gauge eigenstates. In particular, the left-handed light top quark has a non-negligible component of $SU(2)_L$ singlet q_L once M is large. The value of M is constrained by the requirement that the branching ratio of $Z \rightarrow b\bar{b}$ remains consistent with the experiments. It is also constrained by the oblique parameters.

In the CW potential, the M_i^2 is the field dependent squared mass. The constant α is taken to be $-3/2$. Expanding the potential with respect to the physical Higgses, we obtain the SM Higgs potential $V_0(h)$, which determines the SM Higgs vev and its mass, as well as the masses for the other Higgses ϕ^\pm , ϕ^0 , \hat{h}_1^\pm and \hat{h}_2^0 . The orthogonal combination is an exact global symmetry which is preserved by all interactions. Therefore, the corresponding Goldstone boson ϕ^0 remains massless even after spontaneous symmetry breaking. To give mass to ϕ^0 , a μ -term need to be introduced.

In the μ term, to preserve the stability of \hat{h}_2^0 dark matter, we choose $\mu_l = 0$. The second term breaks the $U(1)$ global symmetry that protects the mass of ϕ^0 and thus generates a mass for ϕ^0 . The nonequality between μ_l and μ_r breaks the left-right parity, albeit, only softly. Therefore, it is natural for μ_r to be of the order of f or smaller. μ_r

term also contributes a tree level mass to the SM Higgs. In order not to reintroduce fine tuning, μ_r has to be less than about $\frac{f}{4\pi}$. In our analysis below, we choose μ_r to be fairly small, but enough to push up m_{ϕ^0} above the current experimental bounds.

In the subsections above, we discuss very roughly the individual term in the Lagrangian, and one can refer to Ref. [33] if the particle spectrum and interactions in detail are wanted to be obtained.

Based on the Lagrangian given in Eq.27 and the Eqs.(28-34), we can write, the fermic couplings concerned of our calculation as

particles	vertices	particles	vertices
$W_{+\mu}\bar{t}b$	$e\gamma_{\mu}C_L P_L/(\sqrt{2}s_w)$	$W^{+\mu}\bar{T}b$	$e\gamma_{\mu}S_L P_L/(\sqrt{2}s_w)$
$H\bar{t}t$	$-em_t C_L C_R/(2m_W s_w)$	$H\bar{T}T$	$-y(S_R S_L - C_L C_R x)/\sqrt{2}$
$\Phi^0\bar{t}t$	$-iyS_R S_L \gamma_5/\sqrt{2}$	$\Phi^0\bar{T}T$	$-iyC_L C_R \gamma_5/\sqrt{2}$
$\Phi^+\bar{t}b$	$-i(S_R m_b P_L - yS_L f P_R)/f$	$\Phi^+\bar{T}b$	$i(C_R m_b P_L - yC_L f P_R)/f$

TABLE III: the three-point couplings of the charged gauge boson-fermion and those of the scalar-fermion in the left right twin higgs models. The momenta are assigned according to $V_{\mu}S_1(p_1)S_2(p_2)$. All particles are the mass eigenstates and all momenta are out-going.

AS for the coupling between the boson and the scalars, we find that they all vanish, if we parameterize the scalars in the Goldstone bosons fields as[33],

$$\begin{aligned}
N &\rightarrow \frac{\sqrt{2}\hat{f}}{F(\cos x + 2\frac{\sin x}{x})}\phi^0, & \hat{N} &\rightarrow -\frac{\sqrt{2}f \cos x}{3F}\phi^0, \\
h_1 &\rightarrow 0, & h_2 &\rightarrow \frac{v+h}{\sqrt{2}} - i\frac{x\hat{f}}{\sqrt{2}F(\cos x + 2\frac{\sin x}{x})}\phi^0, \\
C &\rightarrow -\frac{x\hat{f}}{F \sin x}\phi^+, & \hat{C} &\rightarrow \frac{f \cos x}{F}\phi^+.
\end{aligned} \tag{34}$$

where the N , \hat{N} , h_1 , h_2 , C , \hat{C} are in the Goldstone bosons fields,

$$H = i\frac{\sin \sqrt{\chi}}{\sqrt{\chi}} e^{i\frac{N}{2f}} \begin{pmatrix} h_1 \\ h_2 \\ C \\ N - if\sqrt{\chi} \cot \sqrt{\chi} \end{pmatrix}, \quad \hat{H} = i\frac{\sin \sqrt{\chi}}{\sqrt{\chi}} e^{i\frac{\hat{N}}{2f}} \begin{pmatrix} \hat{h}_1 \\ \hat{h}_2 \\ \hat{C} \\ \hat{N} - if\sqrt{\chi} \cot \sqrt{\chi} \end{pmatrix}. \tag{35}$$

By this parameterization, the requirement of vanishing gauge-Higgs mixing terms can be satisfied, i.e, in this redefinition of the Higgs fields, the couplings $WZ\phi^+$, $W\gamma\phi^+$, $WZ_H\phi^+$, $W\gamma_H\phi^+$, $W\phi^0\phi^+$, and $Wh\phi^+$ are zero, which is different with that in the littlest higgs models. The re-parametrization in Eq.34 corresponds to correct unitary gauge choice and are canonically normalized, which has been verified by our rough estimation.

B. LRTH ϕW production at the LHC and the numerical results

Due to the missing of the gauge-Higgs mixing terms, the associated production of the charged scalar ϕ^+ and the charged gauge boson W is different with that in the little higgs models. In Fig. 1, the figures (a) and (e) will not occur in the LRTH models since they contain the guage-higgs mixing couplings, while the others are kept and they are the realization of the ϕW production in the LRTH models.

When discussing the numerical results of the processes, just as the discussions in LH models, we also, firstly, investigate the contributions from every single parton channel, i.e, the gg fusion and the $q\bar{q}$ annihilation processes, respectively, and then sum them for the total contributions.

1. gg fusion in the LRTH models

Different with that of the LH models, the ϕW associated production are carried out only by the box diagrams from gg fusion and t-channel contribution via the quark anti-quark annihilation, just shown as Fig.1 (b)(c) and (d), and the s-channels in Fig.1 (a) (e) are missing.

The production cross sections of the $\phi^+ W^-$ of the gg fusion are plotted in Figs. 8 with $M = 100, 300, 500$ GeV for $\sqrt{S} = 8, 14$ TeV and for $f = 500$ GeV, as functions of the scalar mass m_{ϕ} , assuming the charged and neutral scalar mass degenerate, $m_{\phi^{\pm}} = m_{\phi^0} = m_{\phi^p}$. From Figs. 8, we can see the cross section of this process is less than

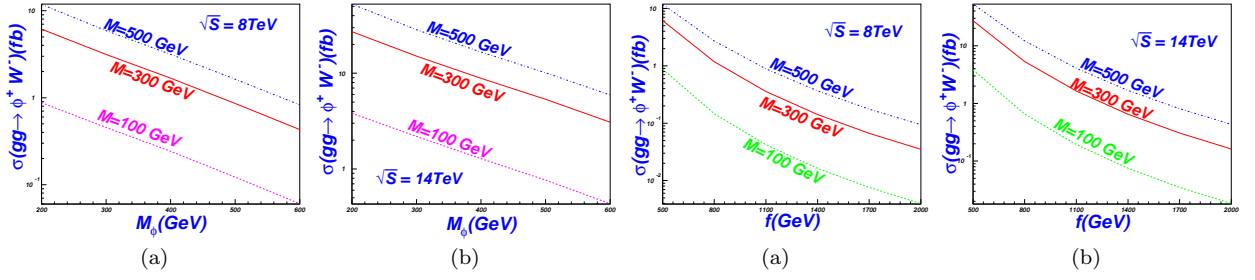


FIG. 8: In LRTH, the cross section σ of the processes $gg \rightarrow \phi^+ W^-$ as a function of the scalar mass m_ϕ or f with $\sqrt{s} = 8$ TeV and $\sqrt{s} = 14$ TeV for $M = 100, 300, 500$ GeV.

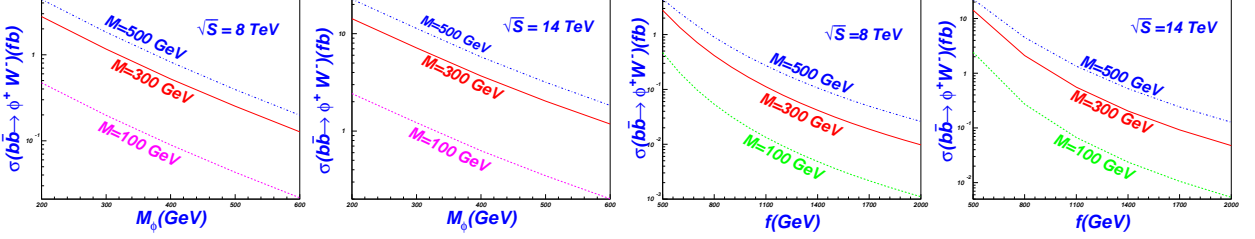


FIG. 9: In LRTH, the cross section σ of the processes $q\bar{q} \rightarrow \phi^+ W^-$ as a function of m_ϕ or f for $M = 150, 250, 500$ GeV with the scalar mass $m_\phi = 200$ GeV and $\sqrt{s} = 8$ TeV and $\sqrt{s} = 14$ TeV.

50 fb in most of the parameter space, even for a larger center-of-mass energy, i.e. at 14 TeV with $M = 500$ GeV. We can also see that, as expected, the production rate decreases with the increasing scalar mass since the phase space are depressed by the mass.

Figs. 8 show the different dependence of the cross sections on the parameter M , with $M = 100, 300, 500$ GeV. The results change with the varying values of M and when M is large, such as

When M is very small, such as $\lesssim 1$ GeV, the collider phenomenology of the $\phi^+ W^-$ will very small, which can be seen clearly via the two group couplings that realize the $\phi^+ W^-$ associated production. The $\phi^+ t\bar{b}$ and $W_\mu^- t\bar{b}$ couplings, for example, are $(S_R m_b P_L - y S_L f P_R)/f$ and $\gamma_\mu C_L P_L / (\sqrt{2} s_w)$, respectively, with $S_L, S_R \sim M/M_T$ and $C_L = \sqrt{1 - S_L^2}$. So when M is small, S_L, S_R will become small too. When $M = 0$, S_L, S_R also change into 0. So if M is too small, the signal will be very small. In the limit case, when $M = 0$, the light top will not mix with the heavy top, so the couplings $\phi^+ t\bar{b}$ disappear, and the contribution are only from the heavy top coupling to the scalar. But the light charged scalar is oppsite, which, mainly coupled to the light top, the heavy top couplings $W^+ T\bar{b}$, proportional to $S_L \sim M$, disappear. So the cross section will drop down to zero when M is in its limit $M = 0$.

We can also see from Figs. 8 that the process $gg \rightarrow \phi^+ W^-$ is dependent strongly on the parameter f , which is understandable since, the most couplings in the LRTH models, such as $\phi^+ t\bar{b}, \phi^+ T\bar{b}$, etc, are tightly connected with the parameter f . The cross sections may be larger unless f is not too high. The rates of the $\phi^+ W^-$ production for $\sqrt{s} = 14$ TeV and $m_\phi = 200$ GeV, for example, are 52 fb and 7 fb, for $f = 500$ GeV and $f = 1000$ GeV, respectively.

2. $b\bar{b}$ annihilation in the LRTH models

Unlike that in the LH models, in LRTH, the ϕW production via quark anti-quark annihilation are realized only by the t-channel parton level $b\bar{b} \rightarrow \phi W$, which is because we have expected the higgs-gauge coupling vanishing, so the s-channel processes are missing, and only the t-channel processes proceeding by the $t - b$ and $T - b$ mixings survive.

Due to the small parton distribution functions, the $b\bar{b}$ realization of the ϕW production, which is tree-level, is not quite large, can arrive at about 20 fb, a little smaller than that of the gg fusion in the loop level realization.

At the same time, we can see that the process $b\bar{b} \rightarrow \phi W$ depends largely on the parameter M and f , and if f goes up, the production rate of this process will decreases, but for parameter M , the cross sections will increase with the increasing parameter M , which can be also seen in Figs. 9.

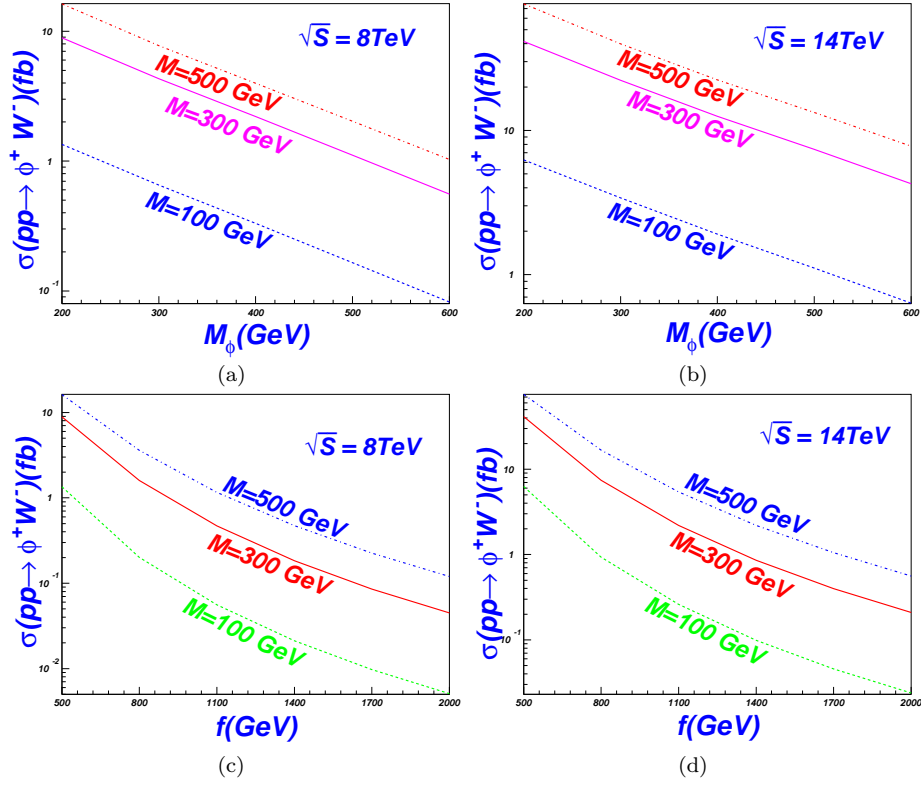


FIG. 10: In LRTH, the total cross section σ of the processes $\phi^+ W^-$ associated production from gg fusion and $b\bar{b}$ collision as a function of the scalar mass m_ϕ or f with $\sqrt{S} = 8$ TeV and $\sqrt{S} = 14$ TeV for $f = 500, 1000$ GeV for different M ($M = 100, 300, 500$ GeV).

3. Total Contribution of the gg and quark anti-quark Annihilation

In LRTH models, we sum all the contribution, from gg fusion and $b\bar{b}$ annihilation for the $\phi^+ W^-$ associated production in Figs. 10, and from which, we can see that the cross section can arrive at tens of fb, dependent on the parameter f , M and the scalar mass in a certain center-of-mass \sqrt{S} . But in quite a large parameter space, the cross sections are less than 10 fb. Normally, at the LHC, this will not interest us, so we will discuss little, also in the following section.

IV. BACKGROUNDS AND DETECTIONS

From the data above, we can see that, at $\sqrt{S} = 8$ TeV, no matter LH or LRTH models, the cross section of the the charged Higgs associated with a W boson production is quite small, even with a little scalar mass, such as 200 GeV, supposing the luminosity to be $10 fb^{-1}$. It is easier, however, for the charged Higgs boson to be observed at $\sqrt{S} = 14$ TeV. Therefore from now on we focus on investigating the charged Higgs associated with a W boson in the following processes at the 14 TeV. The following processes can be considered [35]

$$\begin{aligned}
 pp &\rightarrow W^- H^+ \rightarrow W^- t\bar{b} \rightarrow l^- \nu b\bar{b}jj, \\
 pp &\rightarrow W^+ H^- \rightarrow W^+ t\bar{b} \rightarrow l^+ \nu b\bar{b}jj
 \end{aligned}
 \tag{36}$$

at $\sqrt{S} = 14$ TeV with $200 \leq m_\phi \leq 600$ GeV.

For the processes above with final state $l + \cancel{E}_T + b\bar{b}jj$, the dominant SM backgrounds are $t\bar{t}$, $t\bar{t}W$, $t\bar{t}Z$, $WZjj$, $WWjj$ and $Wjjjj$, which are discussed in Ref. [35]. In the $W^\pm H^\mp$ production processes, four jets are from the charged Higgs decay, and three of them are from top quark decay. Therefore to purify the signal, one can require the invariant mass of final jets to be around the charged Higgs mass, and one top quark is reconstructed by three jets. Since $t\bar{t}$ is one of the predominant backgrounds, one can veto $t\bar{t}$ events if the second top quark can be reconstructed.

The final results given in Ref. [35] show that when after all cuts, there is about 1 fb left for the signal process around $m_{H^\pm} = 500$ GeV, and the backgrounds are suppressed significantly. And Ref. [35] also points out in Table I and II, with the increasing charged scalar mass, the backgrounds become smaller and easier to be depressed, so it seems that the larger the charged scalar mass is, the easier to detect the WH production at the LHC, though the cross section of the signals will also be smaller.

From Ref. [35] Table II, we can see that if the scalar mass is 400 GeV, the S/\sqrt{B} can reach 3.42, and with the increasing m_S (scalar mass), the S/\sqrt{B} gets larger, so we will focus the scalar mass at 400 GeV and larger. From Table I of Ref. [35], we can see if $m_S = 400$ GeV, when the cross section arrive at 49.7 fb, the S/\sqrt{B} will be larger than 3.

Table IV give the optimum value of the ϕ^+W^- production in the LH and the LRTH models at the 14 TeV when $m_\phi = 400$ GeV. The parameters are set as: 1) In the LH models, $s = 0.1$, $s' = 0.5$, $f = 500, 1000$ GeV. 2) In the LRTH models, the involved parameters are $Y = 1$, $f = 500, 1000$ GeV.

LH	x=0.1	x=0.3	x=0.5	x=0.7	x=0.9
f=500	61.45	54.24	70.7	109.7	170
f=1000	21.3	13.3	7.4	3.7	1.24
LRTH	M=0	M=100	M=300	M=500	M=700
f=500	0	1.9	12.5	22.4	29
f=1000	0	0.10	0.86	2.07	3.36

TABLE IV: For $m_\phi = 400$ GeV, the cross section of the signal process at $\sqrt{S} = 14$ TeV for f and M in unit of GeV, cross sections in unit of fb .

From Table IV, we can see that in the LH, when $m_S = 400$ GeV, for the small scale f , the the cross sections are larger than 49.7 fb, the value for the 3σ confidence level. While for the LRTH, it is a little dangerous to reach the detectable level in the most parameter space. In LH models, when f is large, the production rates will be depressed and smaller than 49.7 fb, which will be hardly to probe. The cross sections, however, are also sensitive to the parameters s and s' , this would give quite larger results if we fine tune the parameters. When $s = s' = 0.1$, for example, the production can arrive at 600fb. However, this fine-tuning is not what we want, since it only in a little parameter space and we should consider the confinements such as Ref. [29].

In LH models, however, we can also consider the larger scalar mass, such as 600 GeV, according to Table I and Table II in Ref. [35], the cross sections before cuts is about 14 fb, and the S/\sqrt{B} is 8.77 with the integral luminosity 300 fb^{-1} . We calculate the rate of the ϕW production at $m_\phi = 600$ GeV for $f = 1000$ GeV and $s = 0.1$, we just find that the cross section can arrive at about 9 fb, which is close to 14 fb. So we can image that the signal and backgrounds S/\sqrt{B} should be large, at least larger than 3 for such a large cross section for $m_\phi = 600$ GeV. So we may conclude that for a larger scalar mass, the associated production could be more easily to be detected.

V. CONCLUSION AND SUMMARY

We calculate the charged scalar production associated with a gauge boson W in the LH models and the LRTH realizations. Comparing the two kinds of models, we can see that, at the LHC, the ϕW production in the LH models are larger than that in the LRTH models, and the LH models should be more more possible to be detected at the LHC via the ϕ^+W^- production. From the discussion above, we can also conclude that, in LH models, for a small f , in most parameter space of the LH model, the production rates can arrive at the detectable level. But when f is large, the depression effect becomes strong, so it may difficult for LHC to detect the signal. With a larger scalar mass, however, the signal will be a little easier to detect.

Acknowledgments

This work was supported by the National Natural Science Foundation of China under the Grants No.11105125, No.11105124 and 11205023.

[1] G. Aad et al. (ATLAS Collaboration), Phys. Lett. B **716**, (2012) 1.

- [2] S. Chatrchyan et al.(CMS Collaboration), Phys. Lett. B **716**, (2012) 30.
- [3] C. Quigg, Contemp. Phys. **48**: 1 (2007); S. Matsumoto, M. M. Nojiri and D. Nomurav, Phys. Rev. D **75**: 055006 (2007).
- [4] M. Acciarri *et al.*, [L3 Collaboration], Phys. Lett. B **496**, 200034; ALEPH collaboration, Phys. Lett. B **487**, 2000253.
- [5] LEP Higgs Working Group, hep-ex/0107031.
- [6] A. Abulencia *et al.* [CDF Collaboration], Phys. Rev. Lett. **962006042003**; V. M. Abazov *et al.* [D0 Collaboration], Phys. Lett. B **682**, 2009278; T. Aaltonen *et al.* [CDF Collaboration], Phys. Rev. Lett. **1032009101803**; V. M. Abazov *et al.* [D0 Collaboration], Phys. Rev. D **80**, 2009051107.
- [7] ATLAS Technical proposal, CERN-LHCC-94-38, 254pp. (1994); CMS Technical proposal, CERN-LHCC-94-43, 272pp (1994).
- [8] T. Plehn, Phys. Rev. D **67**, (2003) 014018.
- [9] E. L. Berger, T. Han, J. Jiang, T. Plehn, Phys. Rev. D **71**, (2005) 115012.
- [10] G. P. Salam, Euro. Phys. J. C **67**, 2010637.
- [11] C. K. Vermilion, [arXiv:1101.1335 [hep-ph]].
- [12] A. Abdesselam, E. B. Kuutmann, U. Bitenc, G. Brooijmans, J. Butterworth, P. Bruckman de Renstrom, D. Buarque Franzosi, R. Buckingham *et al.*, Euro. Phys. J. C **71**, 20111661.
- [13] L. G. Almeida, R. Alon and M. Spannowsky, arXiv:1110.3684.
- [14] Shuo Yang, Qi-Shu Yan, JHEP 1202 (2012) 074.
- [15] K. Jakobs, Eur. Phys. J. C **59**: 463 (2009); D. de Florian and M. Grazzini, Phys. Lett. B **674**: 291 (2009).
- [16] A. Cagil, M. T. Zeyrek, Acta Phys.Polon.B42, 45(2011).
- [17] David Lopez-Val, Joan Sola, PoS RADCOR2009 (2010) 045.
- [18] Abdesslam Arhrib, Rachid Benbrik, Chuan-Hung Chen, Rui Santos Phys. Rev. D **80**, (2009) 015010;
- [19] Renato Guedes, Stefano Moretti, Rui Santos, JHEP 1210 (2012) 119.
- [20] Guo-Li Liu, Huan-Jun Zhang, Ping Zhou, JHEP07, (2012)081.
- [21] N. Arkani-Hamed, A. G. Cohen, T. Gregoire, E. Katz, A. E. Nelson, J. G. Wacker, JHEP 0208:021,2002; J. G. Wacker, arXiv:hep-ph/0208235; M. Schmaltz, Nucl. Phys. Proc. Suppl. 117 (2003) 40; M. Schmaltz, D. Tucker-Smith, Ann.Rev.Nucl.Part.Sci.55:229-270,2005.
- [22] Z. Chacko, Hock-Seng Goh, Roni Harnik, Phys. Rev. Lett. **96**, (2006) 231802; Z. Chacko, Y. Nomura, M. Papucci, G. Perez, JHEP 0601:126,2006, Z. Chacko, H. Goh, R. Harnik, JHEP 0601 (2006) 108.
- [23] see e. g., Du Song-Ming, Guo Lei, Liu Wen, Ma Wen-Gan, Zhang Ren-You Phys. Rev. D **86**, 054027 (2012); Ayse Cagil, Huseyin Dag, arXiv:1203.2232; A. Cagil, M. T. Zeyrek, Acta Phys.Polon.B42:45-60,2011; Ayse Cagil, Nucl. Phys. B **843**, 2011(46); Shuo Yang, Phys.Lett.B 675 (2009) 352-355; Qing-Guo Zeng, Chong-Xing Yue, Jiao Zhang, Nucl. Phys. B **860**, 2012(152); Lei Wang, Lei Wu, Jin Min Yang, Phys. Rev. D **85**, 075017 (2012); Yao-Bei Liu, Xue-Lei Wang, Nucl. Phys. B **839**, 2010(294);
- [24] N. Arkani-Hamed, A. G. Cohen, E. Katz, A.E. Nelson, JHEP 0207:034,2002; S. Chang, JHEP 0312 (2003) 057; T. Han, H. E. Logan, B. McElrath, L. Wang Phys. Rev. D **67**, (2003) 095004.
- [25] J. Pumplin, et al., JHEP **0207**, 012 (2002).
- [26] T. Hahn and M. Perez-Victoria, Comput. Phys. Commun. **118**, 153 (1999).
- [27] CDF Collaboration, Phys. Rev. Lett. **105**, 252001 (2010).
- [28] Particle Data Group, J. Phys. G**37**, 075021 (2010).
- [29] Thomas Gregoire, David R. Smith, Jay G. Wacker, Phys. Rev. D **69**, (2004) 115008; C. Csaki, J. Hubisz, G.D. Kribs, P. Meade, J. Terning, Phys. Rev. D **68**, (2003) 035009; M. Chen and S. Dawson, Phys. Rev. D **70**, (2004)015003; S. C. Park and J. Song, Phys. Rev. D **69**, (2004)115010.
- [30] Yao-Bei Liu, Lin-Lin Du, Xue-Lei Wang, Commun. Theor. Phys. **48**, (2007) 699.
- [31] R. Casalbuoni, A. Deandrea, M.Oertel, JHEP **0402**, 032(2004); Chong-Xing Yue and Wei Wang, Nucl. Phys. B**683**, 48(2004); W. Kilian and J. Reuter, Phys. Rev. D**70**, 015004(2004); A. Deandrea, hep-ph/**0405120** 199(2005).
- [32] Z. Chacko, H. S. Goh and R. Harnik, JHEP **0601**, 108 (2006); Hock-Seng Goh, Christopher A. Krenke, Phys. Rev. D **76**, 115018 (2007).
- [33] Hock-Seng Goh, Shufang Su Phys. Rev. D **75**, 075010 (2007).
- [34] Sidney R. Coleman and E. Weinberg Phys. Rev. D **7**, 1888 (1973).
- [35] Shou-Shan Bao, Xue Gong, Hong-Lei Li, Shi-Yuan Li, Zong-Guo Si, Phys. Rev. D **85**, (2012) 075005.